sustainability

MDPI

Article

Potential of Novel Biochars Produced from Invasive Aquatic Species Outside Food Chain in Removing Ammonium Nitrogen: Comparison with Conventional Biochars and Clinoptilolite

Haihong Song [1], Jianming Wang [1], Ankit Garg [1,*], Xuankai Lin [1], Qian Zheng [1] and Susmita Sharma [2]

[1] Department of Civil and Environmental Engineering, Guangdong Engineering Center for Structure Safety and Health Monitoring, Shantou University, Shantou 515063, China; hhsong@stu.edu.cn (H.S.); 18jmwang@stu.edu.cn (J.W.); 13xklin@stu.edu.cn (X.L.); 18zheng3@stu.edu.cn (Q.Z.)

[2] Department of Civil Engineering, National Institute of Technology, Laitumkhrah Shillong 793003, Meghalaya, India; susmita.sharma4@nitm.ac.in

* Correspondence: ankit@stu.edu.cn

Received: 30 September 2019; Accepted: 10 December 2019; Published: 12 December 2019

Abstract: Previous studies for removal of ammonium from wastewater were mainly conducted using biochars produced from agricultural residue. Feedstock type (agricultural residue, wood, animal waste, and aquatic waste), as well as pyrolysis temperature, can significantly influence biochar properties and hence its adsorption capacity. Such studies are useful in decision making for selecting biochar depending on feedstock availability and pyrolysis temperature. This study aims to explore the effects of different types of biochar (laboratory prepared novel water hyacinth and algae biochar, conventional cedar wood, rice straw, and pig manure biochar) on the adsorption kinetics for ammonium removal from wastewater. The adsorption kinetics of biochars were compared to that of commercially available clinoptilolite and interpreted with their respective physicochemical properties (SEM, FTIR, XRD). Batch tests were performed to evaluate the effects of biochars on adsorption of ammonium nitrogen at different concentrations (10 mg/L and 100 mg/L). The tests reveal that clinoptilolite has the highest adsorption capacity. Among biochars, pig manure (animal based) biochar has a higher adsorption capacity in comparison to conventional agricultural residues based biochars. The capacity of pig manure biochar under highly concentrated ammonium solution (100 mg/L) is merely 20% lower than that of clinoptilolite. Both water hyacinth and algae biochar produced at higher temperature (600 °C) show higher sorption rate and capacity (depending on the initial concentration of ammonium) for ammonium in comparison to that produced at a lower temperature (300 °C). This is likely due to an increase in porosity at higher temperatures of pyrolysis.

Keywords: agricultural residue; aquatic species; biochar; ammonium nitrogen adsorption; pyrolysis temperature

1. Introduction

Nitrogen (N) is a critical nutrient required for subsistence of all living organisms [1]. Usage of the nitrogenous fertilizer, in agriculture, is beneficial for plant growth and survival. Ammonium is one such type of nitrogenous fertilizer which is predominantly used in agriculture as a high-N fertilizer. However, in recent years, a substantial amount of ammonium has been deposited into water bodies via agricultural runoff, municipal, and industrial effluent, causing widespread eutrophication of seas,

lakes, and rivers. Therefore, it has become imperative to control the excessive discharge of ammonium into water bodies.

In addition to the conventional biological ammonium removal processes, various other physicochemical or a combination of these methods have been developed to remove ammonium from wastewater, such as membrane filtration [2], ion exchange [3], chemical methods of precipitation [4], biological treatment [5], and adsorption [6]. Among most of these mentioned ammonium removal technologies, adsorption is a promising alternative with a potential to recover and reclaim N for economic and effective land application. Ammonium adsorption is performed using solid porous materials with large surface areas and high affinities to strongly interact with the target material. Various adsorption materials, such as carbon (C) nanotubes, clinoptilolite (a natural material widely recognized for its ammonium adsorption application), and activated C have successfully demonstrated their capability to remove ammonium [7]. However, most of these adsorbents are expensive, have poor adsorption ability, or are not suitable to reclaim N. Therefore, it is necessary to develop novel engineered materials that are highly efficient, cost-effective, and environmentally friendly for the purposes of reclamation of N from wastewater.

Biochar is a porous carbonaceous solid material with a high degree of aromatization and strong anti-decomposition ability that is produced by the thermal decomposition of biomass (e.g. plants and animal waste) under limited oxygen conditions [6–8]. Previous studies have shown that biochar application is a potential sustainable approach for saving irrigation water [9], removal of dimethyl sulfide [10], and soil carbon sequestration [11]. Owing to its large specific surface area, high density of negative surface charges, surface functional groups, adoption of biochar to remove or reduce organic, and inorganic contaminants from water/wastewater, including ammonium has been reported [8]. The molecular structure and the pore size distribution of the produced biochars depend majorly on two factors: (a) the type of feedstock (such as plant-based (wheat, wood, corn, straw, etc.) and animal based (poultry litter, pig manure, etc.)) and (b) pyrolysis conditions (i.e., temperature, heating rate, N flow, and water content) [12–15]. During the process of pyrolysis, biomass undergoes a variety of physical, chemical, and molecular changes which consequently contribute to the adsorption and immobilization of the target contaminant. For instance, biochars produced at higher temperatures tend to possess a larger surface area and porosity compared to the biochar generated at a low temperature range. Such variations may affect the adsorption performance of biochar [13]. Further, the type of feedstock may also influence functions groups present in produced biochar, as different feedstocks are composed of varying degrees of cellulose, hemi-cellulose, and lignin content. Woody biomass pyrolyzed at higher temperature generates a more C-rich biochar compared to non-woody feedstock [16,17]. Also, higher lignin and mineral content in the feedstock results in varying physio-chemical properties of biochar [18].

Research (in literature) demonstrates that most biochars are produced from agricultural residuals [19–22]. On the one hand, agricultural residuals exhibit a great amount of the global production of crop biomass dry matter which are potentially available for biochar pyrolysis [23]. On the other hand, crop biochar application does not only lead to enhanced soil carbon sequestration and plant available nutrients [14,24], but also decreases the toxicity of contaminants in soil [25–28], especially in aqueous solutions [26]. For instance, Gao et al. [20] utilized biochars produced from three different agricultural residuals (cotton stalks, corncobs, and peanut shells) and under three different pyrolysis temperatures (300 °C, 450 °C, and 600 °C, respectively) for the removal of aqueous ammonium. Khalil et al. [22] also analyzed removal of ammonium from fish farms using biochar produced from rice straw. However, though these studies show the potential use of biochar for ammonium removal from aqueous solution, they focused only on biochars generated from agricultural residuals without looking into the possibility of animal waste and aquatic waste biochars that do not compete with food chains. The effect of aquatic species such as *Sargassum horneri* algae and water hyacinth (invasive species commonly found in South China) which have a negligible effect on food chain and animal waste have been rarely utilized for biochar production and ammonium adsorption.

These are available in abundance and considered harmful in nature, and thus utilization of such species for biochar production and its associated ammonium adsorption capacity needs to be investigated.

This study attempts to evaluate the effects of different biochar types (from different feedstocks such as agricultural, wood, animal, and aquatic) on the adsorption kinetics for ammonium removal from wastewater. The feedstocks were selected based on their commonality in literature (rice straw, cedar wood, and pig manure), as well as availability in east coast region (Shantou) of China (for aquatic species such as water hyacinth and *Sargassum horneri*). Biochars from aquatic species do not usually compete with the food chain, unlike agricultural residues, which have an alternative use in feeding animals on small farms in mainly agrarian economies. Further, the effect of pyrolysis temperature was also investigated for laboratory prepared biochars derived from aquatic species at 300 °C (low temperature biochar) and 600 °C (high temperature biochar), respectively. Adsorption kinetics of ammonium for biochars and micro-structural analysis were also compared with that of commercially obtained clinoptilolite. Elucidation of the effect of the pyrolysis conditions and the type of feedstock on adsorptive capacity of biochar for ammonium will be helpful in providing basic information to support a detailed understanding of the biochar interaction with contaminants for the preliminary design of bio-filtration systems for removal of ammonium from wastewater.

2. Materials and Methods

2.1. Production of Biochars from Aquatic Species Outside Food Chain and at Different Pyrolysis Temperatures

The materials used for the present study included (a) three commercially available biochars; namely, pig manure biochar, cedar biochar, and rice straw biochar; (b) four laboratory produced biochars; namely, water hyacinth and *Sargassum horneri* algae at two different pyrolysis temperatures; and (c) one commercial clinoptilolite. The three commercial biochars were purchased from Jinguo Boiler Company, China. According to the specifications provided by the manufacturer, pig manure biochar was produced by heating pig manure mixed with rice husk particles at 600 °C; cedar biochar was produced by heating cedar at 750 °C, and rice straw biochar was produced by heating compressed rice straw at 600 °C, each for a heating time of 10 min and under a low oxygen environment. Costs of rice straw biochar, pig manure biochar, and cedar wood biochar as provided by supplier were approximately 0.86 USD, 0.87 USD, and 0.43 USD per kg, respectively. The cost of clinoptilolite (0.46 USD per kg) was slightly higher than that of cedar wood biochar and lower than other biochars.

For laboratory produced biochars, the protocols as mentioned by Bordoloi et al. [20] were adopted. Water hyacinth plants, an abundant cellulose biomass, and *Sargassum horneri* algae, an abundant carbohydrate biomass were the precursors for biochar preparation. The feedstocks were washed under clean tap water, sliced into pieces, and sundried for 4–5 days until the stem color changed from green to brown. Dry water hyacinth and algae samples were separately processed through a fixed bed pyrolysis reactor (OTF-1200X-100 Hefei Kejing) under 300 °C and 600 °C, respectively (refer to Figure 1), and at a fixed pyrolysis time of 180 min. The carbonization process was conducted under low oxygen conditions by covering both sides of the tube furnace (with an alundum combustion boat of 90 mm × 90 mm × 30 mm) through an air valve and a constant heating time of 10 °C/min. Each time, 3–4 gram of biochar was produced. The commercial clinoptilolite (particle size 2–3 mm) was purchased from Liaoning Province in Northeast China. More details of the biochars investigated can be referred to in Table 1.

Table 1. Characteristics of different adsorbents.

Biochar	Pyrolysis Temperature (°C)	BET Surface Area(m^2/g)	Pore Volume (cm^3/g)	Average Pore Diameter (nm)	References
Clinoptilolite	450	84.45	0.053	2.51	[29]
Pig manure	350	23.8	0.053	8.83	[19]
Pig manure	700	32.6	0.035	4.26	[19]
Rice straw	224	31.6	0.042	5.2	[30]
Cedar wood	460	259	0.088	21.1	[31]
Sargassum horneri	700	34.426	0.043	2.503	[32]
Water hyacinth	700	36.16	0.047	5.21	[33]
Water hyacinth	300	4.77	0.201	16.83	[33]

For laboratory prepared biochars, the cost was calculated by combining expenditure incurred for 1) Extracting (labor cost of 2 USD per kilogram of Water hyacinth and Algae); 2) Transportation cost (0.3 USD) from water body to Laboratory at Shantou University; 3) Processing of both aquatic species in laboratory, and 4) Pyrolysis process (mainly electricity cost of 24 USD). Total cost for production of biochar of 1 kg from aquatic species was approximately 26.3 USD. The cost was significantly higher as compared to commercially purchased biochars, which were produced at a much larger scale. For the current study, which was conducted at a very small scale (0.105 kg of biochar required), it is therefore not scientific to conduct any cost comparison. Further systematic studies are required in the direction of cost comparison of production of biochar from different feedstocks considering its scale.

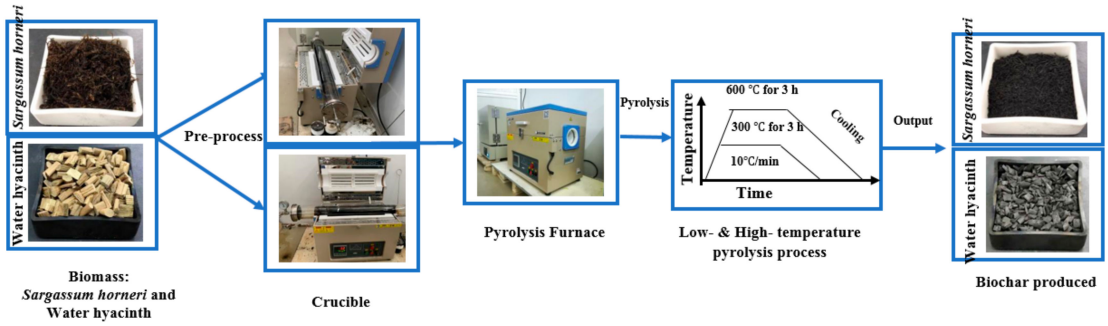

Figure 1. Overview of newly laboratory prepared biochars from aquatic species in this study at two different pyrolysis temperatures (300 °C and 600 °C). Apart from these biochars, three other biochars (pig manure, cedar wood, rice straw) and commercially used clinoptilolite were utilized in this study for adsorption of ammonium.

2.2. Characterization of Laboratory Prepared Produced Biochars and Clinoptilolite.

The microscopic structures of the adsorbents were analyzed by a high-resolution scanning electron microscope (SEM) (Gemini 300, Carl Zeiss AG, SEM) with an acceleration of 0.5 and 1KV. X-ray power diffraction (XRD) analysis was performed using a computer-controlled X-ray Diffractometer (D8 ADVANCE, Bruker) equipped with a stepping motor and graphite crystal monochromator, at a scanning rate of 0.02°/sec for 2θ ranging between 5 to 50°. Infrared spectra of the biochar were recorded on a Fourier transform infrared spectrometer (Nicolet6700, Somerfield, FTIR). The FTIR spectrum was recorded over a wavenumber range of 4000–800 cm^{-1}, with 32 scans performed, under a spectral resolution of 4 cm^{-1} (details of the methods can be referred to Garg et al. [34] and Kumar et al. [35])

2.2.1. Morphological Properties of the Materials

Figure 2a–h shows the SEM micrographs of biochars at two magnifications (i.e., 500×, 1000×). SEM images of pig manure biochar (Figure 2b) display a large porous and foam-like structure (but the greater size particles may result in lower surface-to-volume ratio in the biochar). Cedar wood biochar (Figure 2d) shows a layered structure in accordance with water hyacinth and algae biochar (Figure 2e,f) at 300 °C. The planar cleavage and smoothened surface of the water hyacinth and algae biochar may

be due to volatilization of all hydrocarbons. The effect of temperature can be clearly seen in biochars produced from water hyacinth (Figure 2e–g) and *Sargassum horneri* algae (Figure 2f–h). As observed, the rise in temperature will result in carbonization of biomass, that will in turn result in a release of volatile matter from char generating higher pores and surface area. Thus, the biochar produced at 600 °C can be seen to be further inerratic and flat, in comparison to the biochar produced at lower temperature, with several micro pores on the surface, demonstrating an increase in surface area and thereby providing additional sites for adsorption, nutrients, and water retention. Rice straw biochars (refer Figure 2c) have a small pyramidal (hollow and porous) structure, with a high surface-to-volume ratio making it suitable for high adsorption.

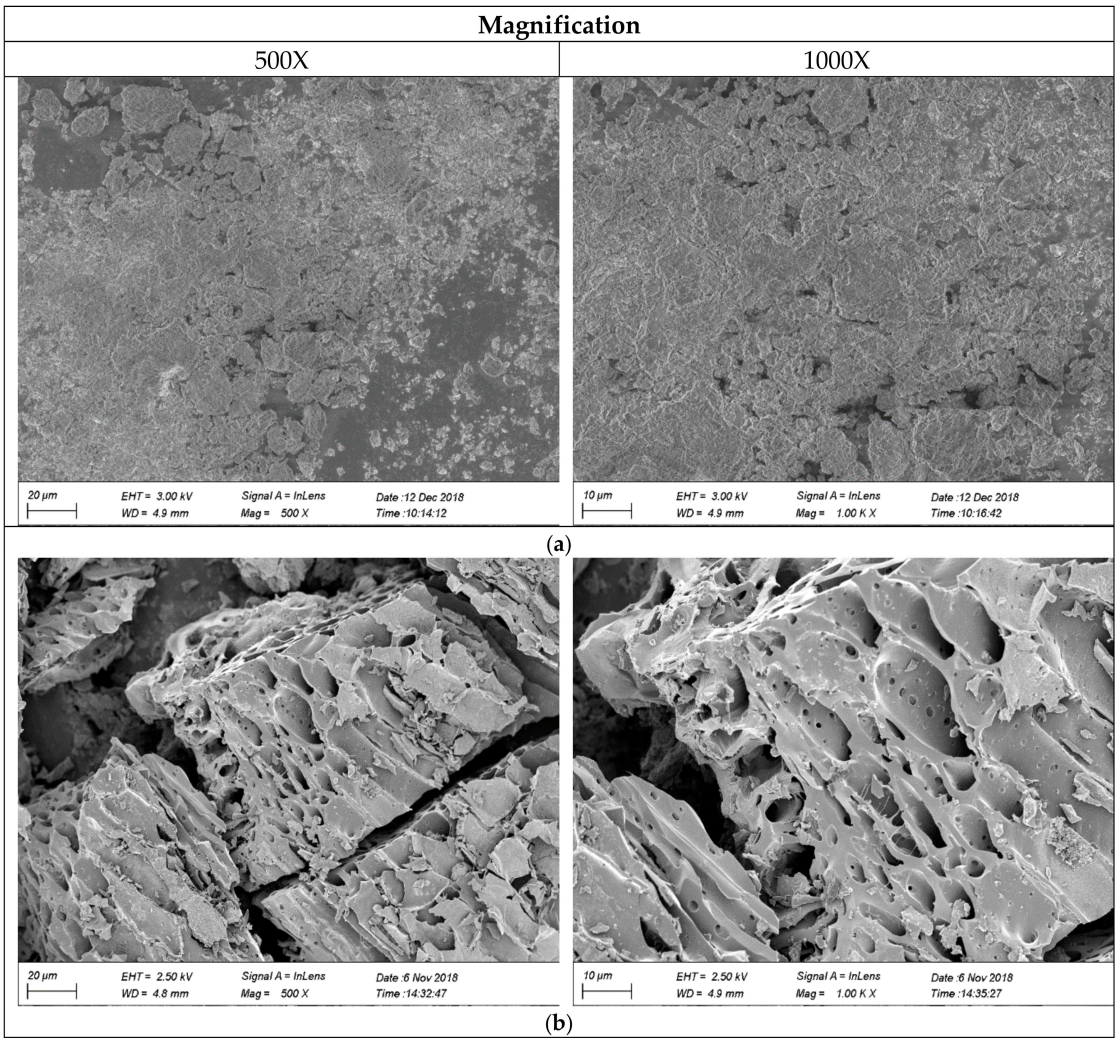

Figure 2. *Cont.*

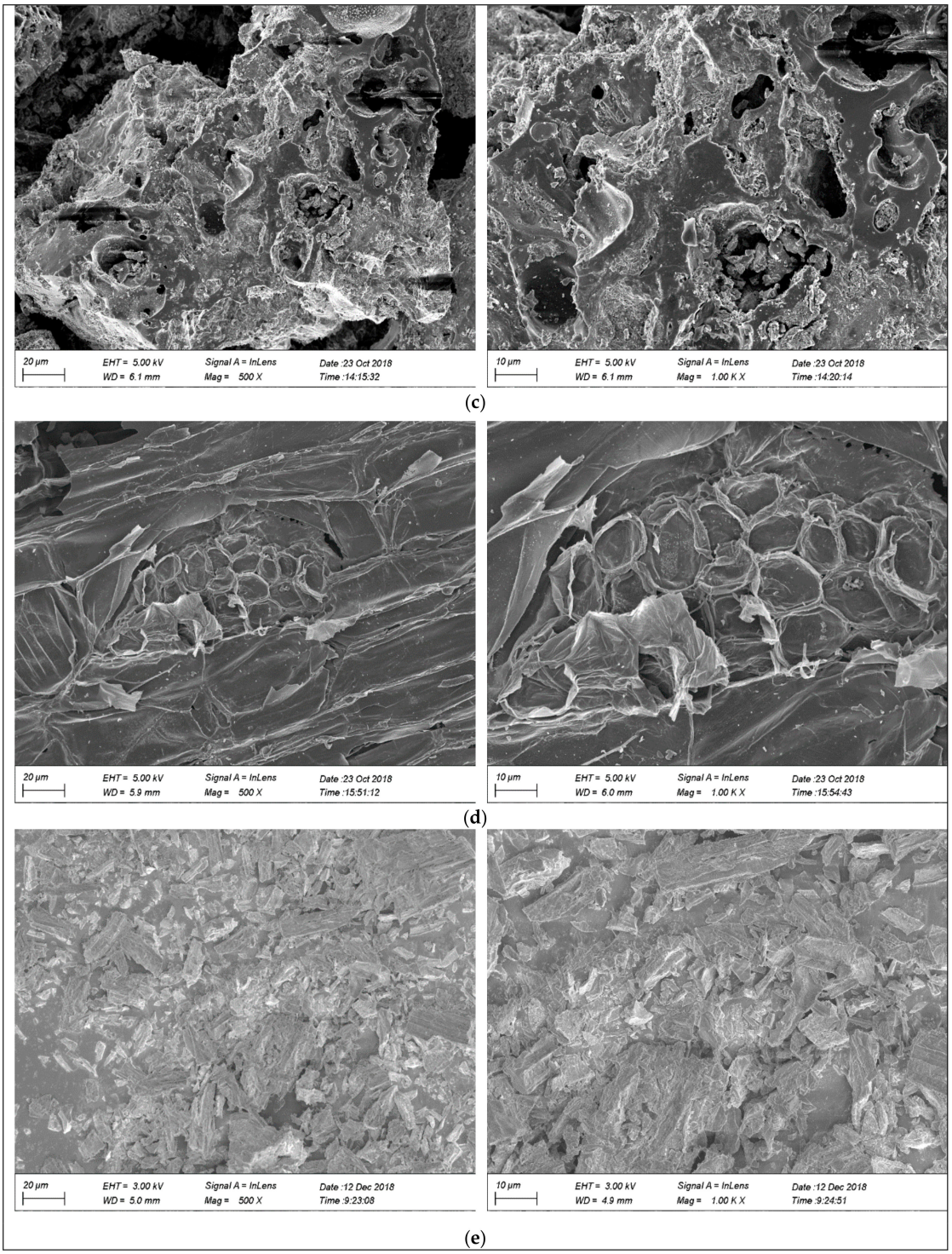

Figure 2. *Cont*.

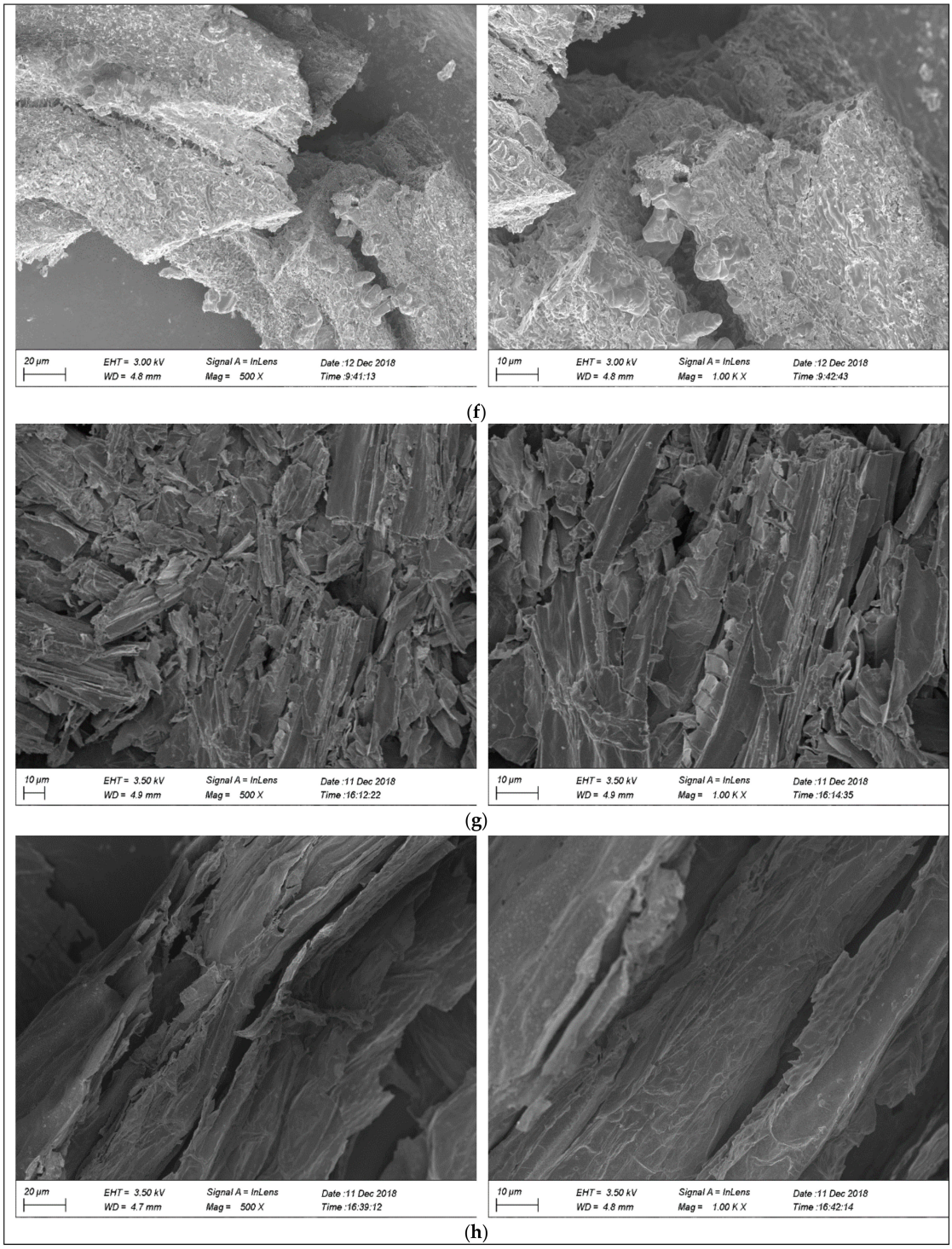

Figure 2. Scanning electron microscope (SEM) images of (**a**) Clinoptilolite; (**b**) pig manure biochar; (**c**) rice straw biochar; (**d**) cedar wood biochar; (**e**) water hyacinth biochar (300 °C); (**f**) *Sargassum horneri* biochar (300 °C); (**g**) Water hyacinth biochar (600 °C); (**h**) *Sargassum horneri* biochar (600 °C).

On the other hand, clinoptilolite (Figure 2a) appears to have large tabular crystals with a porous structure, smaller particle size, and high silica content that will result in a higher surface area and porous characteristics.

2.2.2. Atomic and Molecular Structures of the Materials

Figure 3a–h shows the XRD patterns of all the adsorbents. As evident from the figures, the characteristic peak at 2θ = 26.7° and 29.3°, displayed for all the adsorbent types, corresponds to Quartz and Calcite, respectively. Calcite and quartz are the most commonly found minerals in biochar due to carbonation of Ca oxide. The peaks at 2θ = 28.3°, 31.3°, and 40.4° in the case of pig manure and rice straw biochar represents Whitlockite mineral due to the presence of phosphate in the feedstock. The presence of calcite is probably due to high Ca content found in the pig manure feedstock due to pig diets. For rice straw biochar, additional Quartz peaks are displayed at 2θ = 20.9°, 26.6°, and 39.5°, demonstrating its crystalline behavior. Sylvite peaks are located at 40.7° in the case of rice straw biochar and aquatic biochars for both temperatures of pyrolysis (300°C and 600°C). In contrast, wood biochar does not display any peak, hence confirming its amorphous nature. However, the commercially obtained clinoptilolite displayed its crystalline nature with the existence of Quartz peaks with 2θ at 9.8°, 11°, 13°, 17.3°, 18.7°, 22.2°, 26.6°, 29.9° and31.9°. This observation is in coherence with the FTIR spectrum (Figure 4) which confirms the main components of clinoptilolite to be SiO_2 and Al_2O_3.

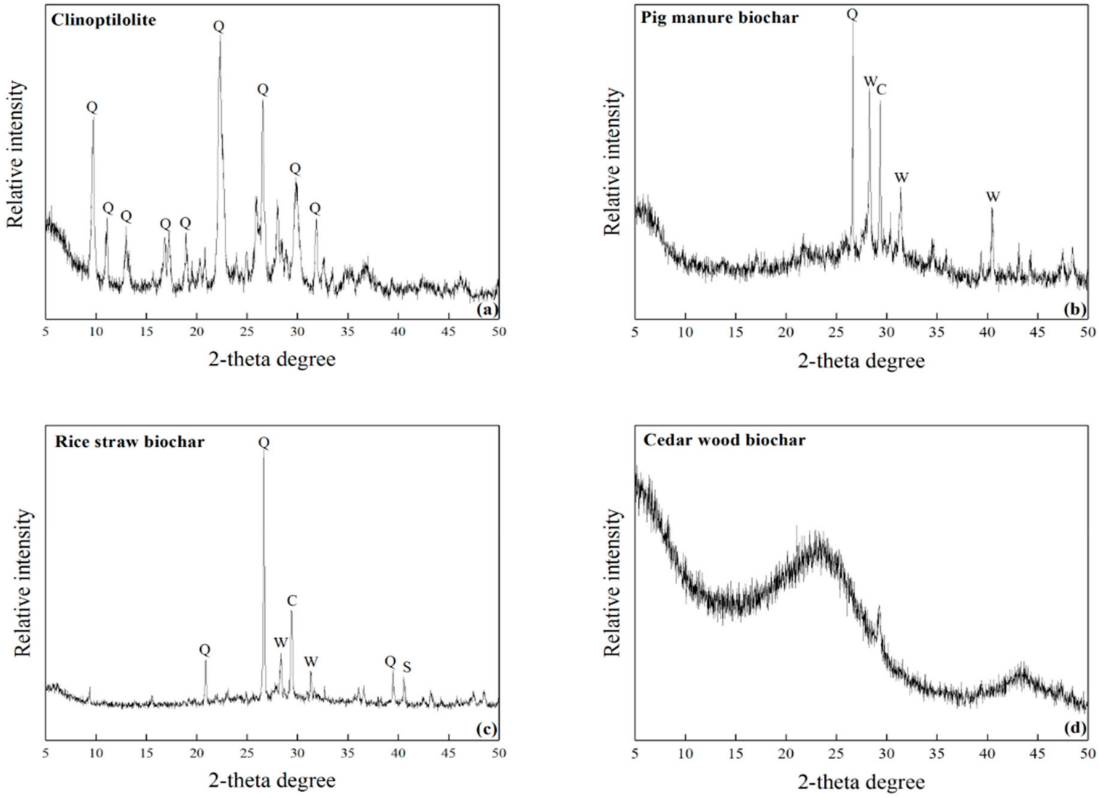

Figure 3. *Cont.*

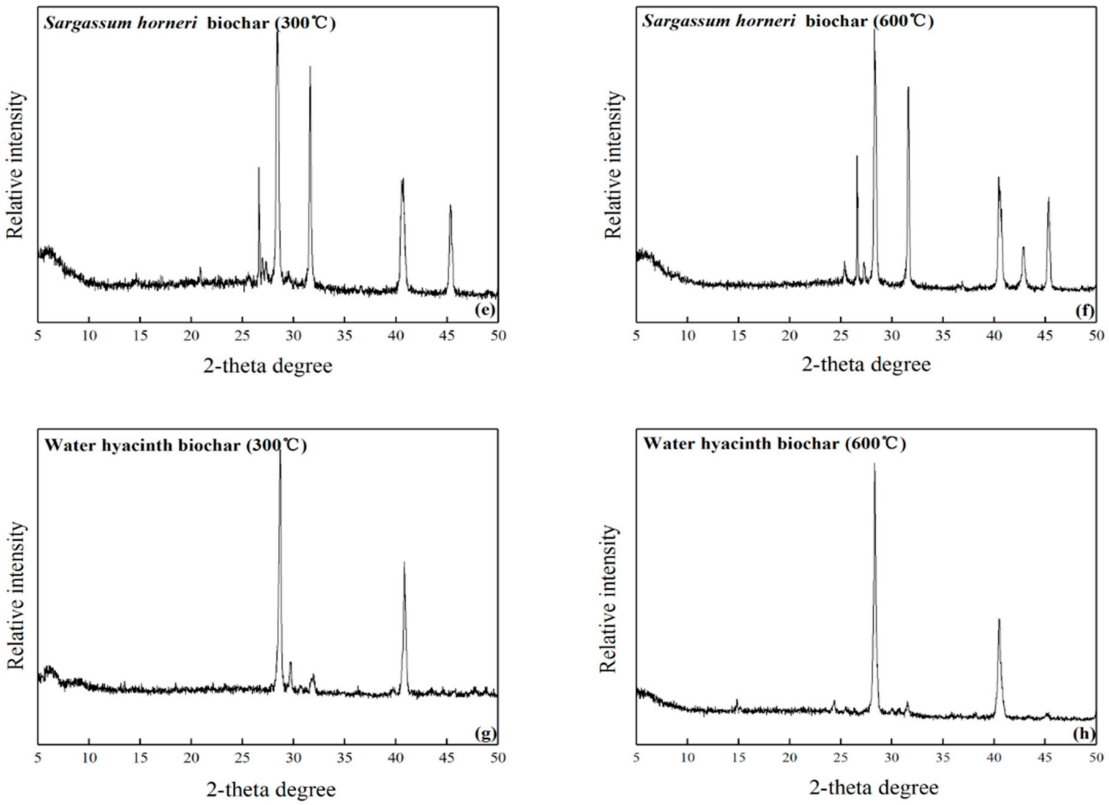

Figure 3. The XRD results of (**a**) Clinoptilolite; (**b**) Pig manure biochar; (**c**) Rice straw biochar; (**d**) Cedar wood biochar; (**e**) Sargassum horneri (300 °C); (**f**) Sargassum horneri (600 °C); biochar; (**g**) Water hyacinth (300 °C); (**h**) Water hyacinth (600 °C) (Q = Quartz, C = Calcite, S = Sylvite, W = Whitlockite).

2.2.3. Chemical Structure of Clinoptilolite and Biochar

The Fourier Transform infrared spectroscopy (FTIR) spectra of selective biochars (as some biochars did not show peaks) and clinoptilolite are shown in Figure 4a–d. FTIR spectroscopy can provide direct information on the existence of different surface fractional groups present in the organic matter of biochars. For pig manure biochar (refer Figure 4a), the strongest peak position is observed near 1039 cm^{-1}, 875 cm^{-1} and 1417 cm^{-1}. This can be attributed to C-O stretching, aromatic C-H and C = C aromatic stretching, respectively. The peaks at 875 cm^{-1} and 1417 cm^{-1} are indicative of calcite, which are in agreement with the XRD analysis. However, in Figure 4b, the peak position in the FTIR spectra of wood biochar seems to be unclear, implying that there is mainly presence of amorphous C along with the absence of C-O and C-H groups; hence, humidity and lower carbon content. The figure of wood biochar is consistent to its XRD result. The FTIR spectra of rice straw biochar (refer Figure 4c) is very similar to that of pig manure biochar with broad bands centered at 874 cm^{-1}, 1088.3 cm^{-1}, 1610 cm^{-1} and 3411 cm^{-1} representing stretching of aromatic C-H, C = O, C = C, and −OH, respectively. The occurrence of the bands at 874 cm^{-1} can also be due to an increasing degree of condensation of organic compounds in the biochar. FTIR (refer Figure 4d) of clinoptilolite shows broad band at 3500–3300 cm^{-1} and 1600–1650 cm^{-1} illustrating discrete water absorption bands attributed to –OH bonds or phenolic groups. From Figure 4, it can be further concluded that clinoptilolite has TO_4 (T = Si and Al) (stretching at 1036 cm^{-1}) as well as C = O (stretching at 1730 cm^{-1}) [36]. From the FTIR results, it is observed that rice straw biochar and clinoptilolite have aromatic C compounds and moisture. Peak shifting is observed to the lower wavenumber for pig manure, which shows an increase in mass of the C = O molecule in comparison to straw biochar. This is because frequency of vibration is inversely proportional to mass of the vibrating molecule; hence, the lighter the molecule is, the higher vibration frequency and wave numbers, revealing pig manure biochar has higher aromatic content than straw biochar samples.

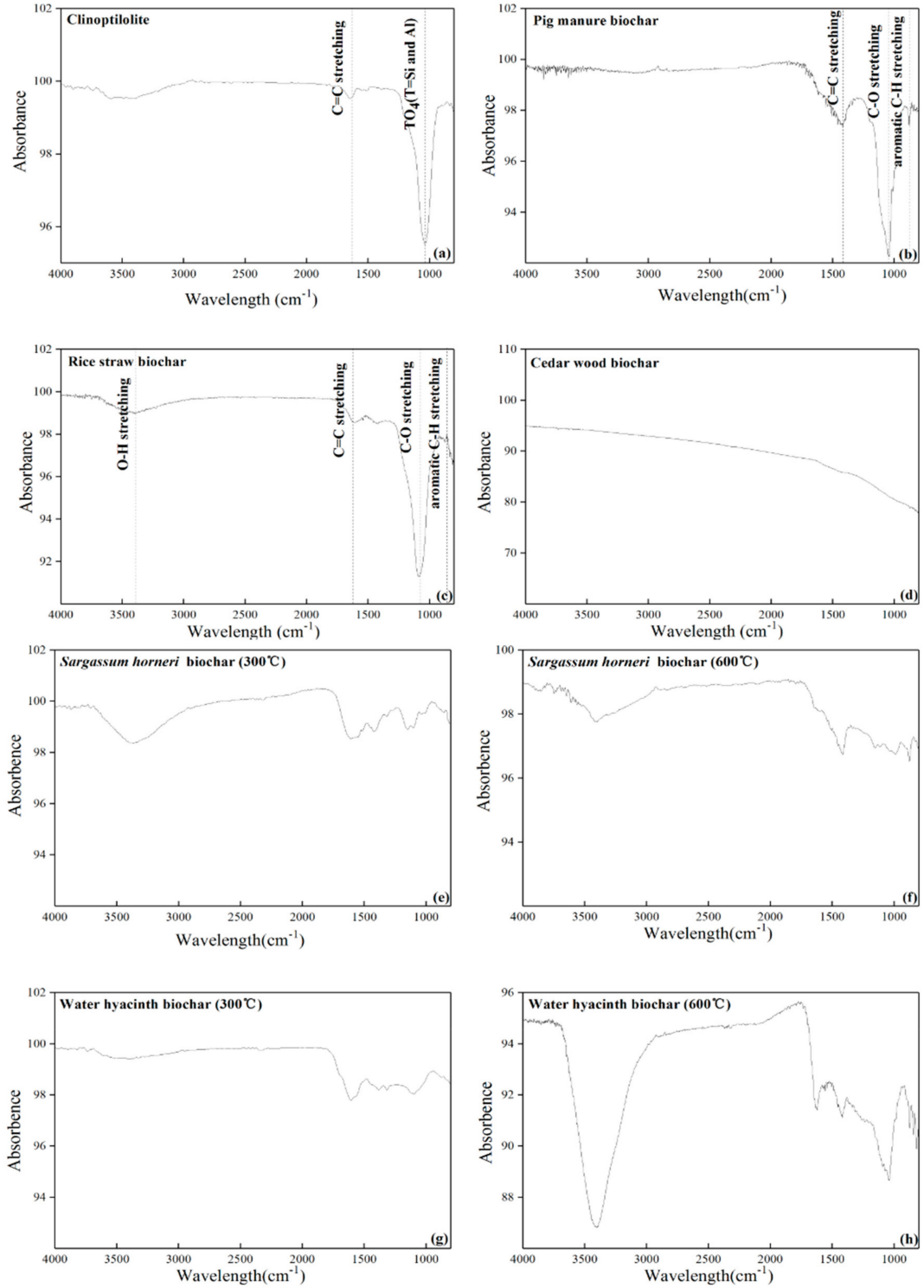

Figure 4. FTIR spectra of (**a**) Clinoptilolite (**b**) pig manure biochar; (**c**) rice straw biochar; (**d**) cedar wood biochar; (**e**) Sargassum horneri (300 °C) biochar; (**f**) Sargassum horneri (600 °C) biochar; (**g**) water hyacinth (300 °C) biochar; (**h**) water hyacinth (600 °C) biochar.

2.3. Testing Procedure for Batch Experiments.

Adsorption kinetics: 5 g of each biochar was mixed with 50 mL ammonium solution prepared at two different concentrations (i.e., 10 mg/L and 100 mg/L) and the adsorption kinetics of ammonium was analyzed. The Erlenmeyer flasks (250 ml, used for preparation of ammonium solution) were covered with plastic film for minimizing evaporation. The flasks were then immediately placed in a

constant temperature shaker (25 ± 0.5 °C) and shaken at 150 rpm for uniform mixing of biochar with the ammonium solution. 1 mL of the suspension was taken from each flask at different time intervals i.e., 0 to 240 min, for analysis of Total Ammonium Nitrogen (TAN) concentration in the remaining solution. TAN was measured using a UV-visible spectrophotometer 752 (Spectrum Instruments, China) following the colorimetric procedure as described by [37]. All samples were tested against their absorption prior to reagent addition. The adsorbed TAN concentrations on all material samples were calculated based on the difference between the liquid phase initial prior to biochar addition and final TAN concentrations. The experimental treatments trials were performed in three replicates and average value is reported.

Adsorption isotherms: The adsorption isotherm of ammonium onto the biochar was attempted by mixing the biochar at different dosages (i.e. 10, 20, 50, 80, 100, 120, and 150 mg/L) with 250 mL of different concentrations of ammonium solution in Erlenmeyer flasks. The flasks were shaken on the constant temperature shaker (25 ± 0.5 °C) at 150 rpm for 240 min. Water samples were then withdrawn to measure the TAN concentration with the method mentioned above. A pH of 7 was maintained throughout the tests, as it was found to be the most optimal range of adsorption efficiency [22].

The ammonium uptake (Qe) was calculated using the following equation:

$$Q_e = \frac{(C_0 - C_e)V}{M} \quad (1)$$

where,

Q_e—the amount of total adsorbed ammonium (mg/g)
C_0—initial concentrations of ammonium in solution (mg/L)
C_e—equilibrium concentrations of ammonium in solution (mg/L)
V—the solution volume (L)
M—the adsorbent weight (g)

The fitting parameters of Lagergren pseudo-first order kinetics, pseudo-second order kinetics and Langmuir isotherm were obtained using the cftool function in Origin 8.0 software (OriginLab Corp, USA). Adsorption kinetics of ammonium were described from both pseudo-first-order model as Equation (2) and pseudo-second-order model as Equation (3):

$$\ln(Q_e - Q_t) = \ln Q_e - k_1 t \quad (2)$$

$$\frac{t}{Q_t} = \frac{1}{Q_e^2} k_2^{-1} + \frac{t}{Q_e} \quad (3)$$

where,

k_1—the rate constant of pseudo-first order (min^{-1})
Q_t—adsorption capacity of nitrogen at interval time of t (mg/g)
k_2—the rate constant of pseudo second order (g/(mg·min))

Adsorption process of nitrogen was described by Langmuir model as Equation (4)

$$\frac{C_e}{Q_e} = \frac{1}{Q_{max} k_L} + \frac{C_e}{Q_{max}} \quad (4)$$

Q_{max}—the maximum adsorption capacity of nitrogen (mg/g)
k_L—the Langmuir constant (L/g)

3. Results and Discussion

3.1. Ammonium Adsorption Kinetics of Different Adsorbents

Dynamics of Ammonium Nitrate adsorption in 10 mg/L and 100 mg/L are presented in Figues 5 and 6, respectively. The experimental results were fitted to the kinetic models of pseudo-first order and pseudo-second order as given in Figures 5 and 6. The pseudo-second order model is most acceptable in describing adsorption kinetics of nitrates on biochar [19,38]. As observed in the figures, it can be highlighted that the rate of adsorption takes place in two phases; for the initial phase within retention time up to 200–300 min, about 60–70% of the adsorption is completed (for all the studied adsorbents) and the later phases, remaining adsorption takes place until it reaches an equilibrium state. Higher adsorption rate in the beginning can be due to initial accumulation of ammonium on the surface of biochar during the first 240 min. After initial accumulation, the surface of biochar tends to be saturated with ammonium, thereafter, causing repulsion of further ammonium ions. This trend is consistent with the studies obtained by Gao et al. [20] and Khalil et al. [22]. However, the adsorption capacity (Qe) values obtained in the present study are much lower (in an order of 10 times) than that observed by Gao et al. [20], which may be due to variation in the testing conditions of feedstock. Gao et al. [20] and Khalil et al. [22] utilized biochar from crop residues (cotton stalks, corncobs, and peanut shells), along with very high ammonium concentration of 500 mg/L mixed with NaCl. However, Qe values of the current study are comparable with the results obtained by Zhang et al. [19], where biochar was generated from raw corn and tested for its adsorptive capacity for ammonium solution of up to 160 mg/L. Natural clinoptilolite has exhibited the highest adsorption capacity (Qe = 0.38 mg/g) compared to all biochars utilized in this study, which may be due to deprotonating of carboxyl and phenolic groups or precipitation of the free aluminum as oxides, resulting in the negatively charged organic groups serving as the adsorption sites for ammonium [39,40]. However, the adsorption capacity of clinoptilolite in 100 mg/L ammonium solution was more than 6 times that in the solution of 10 mg/L ammonium. The trend is similar for biochars as well, but the differences in their adsorption capacity vary as compared to clinoptilolite. This seems to suggest that for maximizing efficiency of any adsorption material to be used in a biofilter system, it is important to understand the concentration of ammonium in an incoming effluent.

Among all biochars, pig manure (from animal waste) seems to have the highest adsorption capacity (0.2 mg/g), followed by rice straw biochar (0.09 mg/g) and cedar wood biochar (0.08 mg/g). Khalil et al [21] explored utilization of one type of biochar from rice straw (activated using soaking with NaOH) for adsorption of ammonium from fish wastewater. Their study found that rice straw biochar shows adsorption capacity ranges from 1–4.5 mg/g for concentration of ammonium solution up to 25 mg/L. The studies undertaken by Khalil et al. [22] produced activated biochar, with necessary pre-activation process, was not the same in case of the commercially available biochar used in the study. Lower values of ammonium adsorption in the present study could be due to differences in the biochar activation process. The laboratory produced biochars from aquatic species such as water hyacinth and algae showed least adsorption capacity (< 0.8 mg/g). The reason for this is probably due to a lack of carboxyl ((C = O) and OH—groups in plant-based biochars (wood and aquatic species) as compared to pig manure. Further, there is also a lower density of quartz in cedar wood as well as algae/water hyacinth biochars as compared to pig manure. This explains the reason of least adsorption rate in the case of cedar wood, algae, and water hyacinth biochars. Interestingly, aquatic species biochars produced at a higher pyrolysis temperature (600 °C) show consistently higher adsorption capacity in the beginning (~ 50 %), but their difference becomes negligible at equilibrium. This shows that the rate of adsorption is faster in biochar produced at higher temperatures. The result is in contrast to a study by Gao et al. [20] where biochars produced from low pyrolysis temperature (obtained from crop residues such as cotton stalks, corncobs and peanut shells) shows faster sorption rate or higher adsorption capacity, in the presence of NaCl added to ammonium solution. Additionally, it can be understood

that depending on the feedstock (crop residue or aquatic species) composition, i.e. cellulose, lignin, and hemi-cellulose content, the quality of the produced biochar can vary significantly [41,42].

The pyrolysis (mainly cellulose and hemi-cellulose) at a lower temperature of around 400 °C can lead to release of aliphatic and labile compounds whereas, pyrolysis (mainly lignin) at higher temperatures (> 500 °C) can lead to release of carbon dioxide, ethylene, and ethane [43]. Therefore, biochar produced mainly at lower temperature may not be fully charred and may contain mobile organic compounds [44]. These mobile organic compounds can be released during leaching and may lead to toxic effects [43]. Yao et al. [45] also investigated effects of various biochars from peanut hull, Brazilian pepperwood, sugarcane bagasse, and bamboo on adsorption and leaching of ammonium. It was found that biochars produced at a higher pyrolysis temperature (~ 600 °C) are likely to reduce leaching of nutrients. In the current study, however, no signs of leaching from biochars was observed during the testing period. It is suggested that long-term studies need to be conducted for biochars (especially produced at lower temperature of 300 °C) in order to explore possible leaching effects.

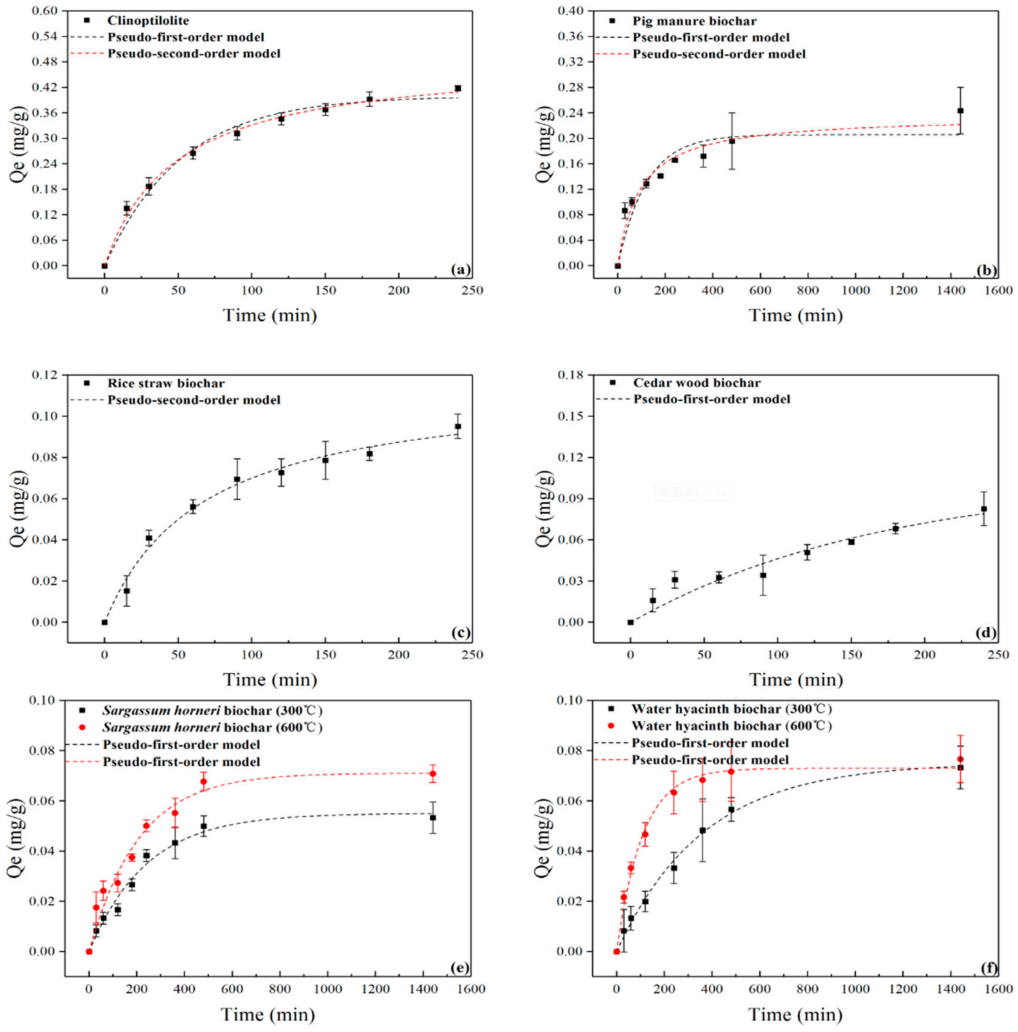

Figure 5. Adsorption kinetics curves of different adsorbents such as (**a**) Clinoptilolite; (**b**) Pig manure biochar; (**c**) Rice straw biochar; (**d**) Cedar wood biochar (**e**) *Sargassum horneri* (300 °C) and *Sargassum horneri* (600 °C) biochar; (**f**) Water hyacinth (300 °C) and Water hyacinth (600 °C) biochar in initial 10 mg/L ammonium solution.

Interestingly, the adsorption capacity of pig manure rises to around 2 mg/g (~9 times) in an ammonium solution of 100 mg/L (Figure 6). The adsorption capacity of pig manure is only 20% lower than that of clinoptilolite. Rice straw biochar also possesses higher adsorption capacity (1.4 mg/g;

Figure 6) in a solution of 100 mg/L. For other biochars such as water hyacinth and algae, the effect of an increase in concentration of solution seems to be lower, suggesting that the effect of an increase in concentration of ammonium solution is higher in pig manure and straw biochars. By comparing Figures 5d–e and 6e–f, it was noticed that the effect of a difference in pyrolysis temperature (300 °C and 600 °C) increased significantly with an increase in ammonium concentration (from 10 mg/L to 100 mg/L). However, towards equilibrium, the difference can be noticed only for water hyacinth biochar and not for algae biochar. It is reasonable to confirm that pyrolysis temperature has more influence on the sorption rate than its capacity (at equilibrium) in both types of biochar. The further investigation, on comparison of the characteristics of the pristine materials before and after the adsorption (Figure 7) revealed clear change in peaks as observed in an FTIR analysis for both clinoptilolite and rice straw biochar, indicating that adsorption has taken place.

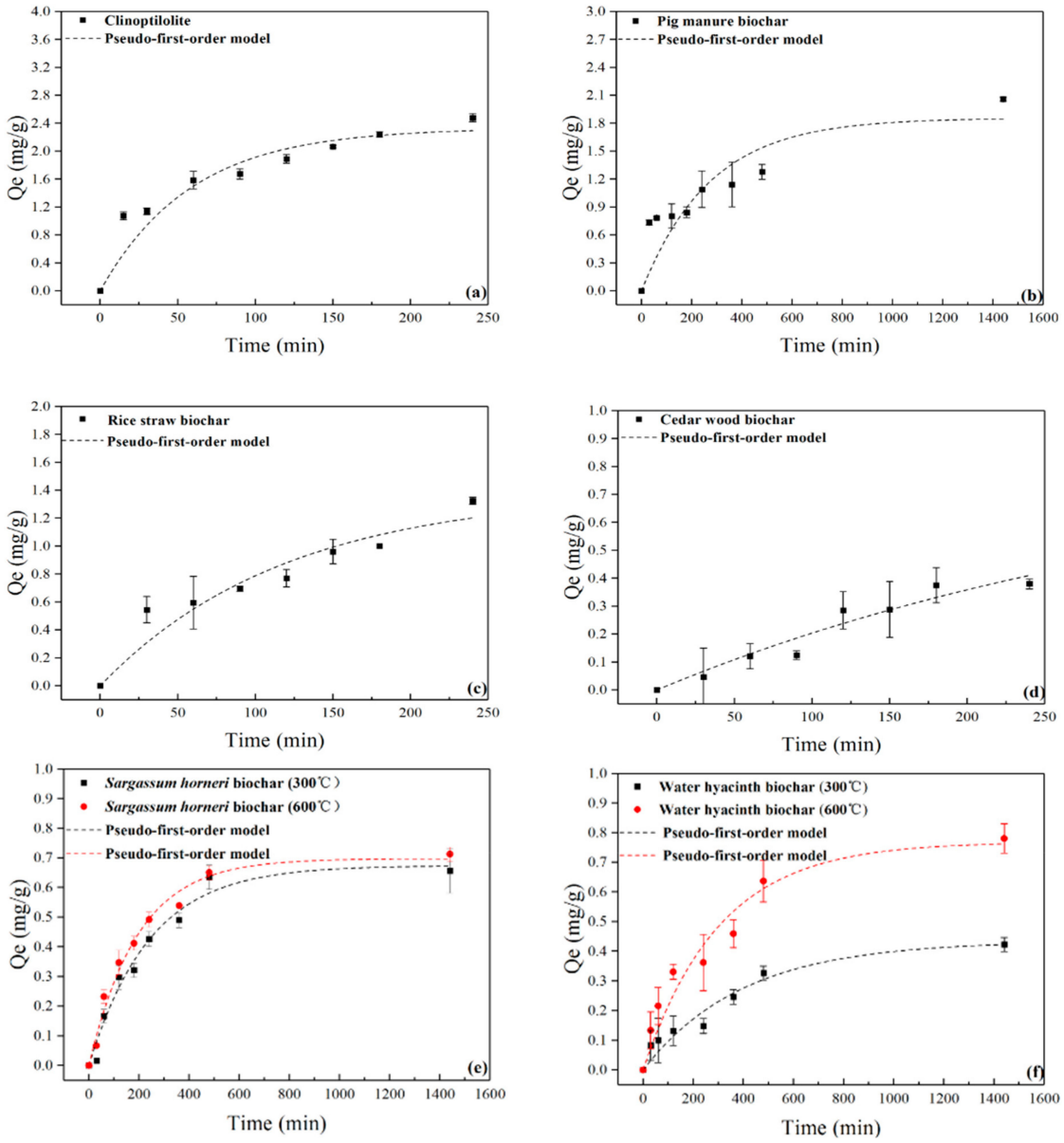

Figure 6. Adsorption kinetics curves of different materials such as (**a**) Clinoptilolite; (**b**) Pig manure biochar; (**c**) Rice straw biochar; (**d**) Cedar wood biochar; (**e**) *Sargassum horneri* (300 °C) and *Sargassum horneri* (600 °C)biochar; (**f**) Water hyacinth (300 °C) and Water hyacinth (600 °C) biochar in initial 100 mg/L ammonium solution.

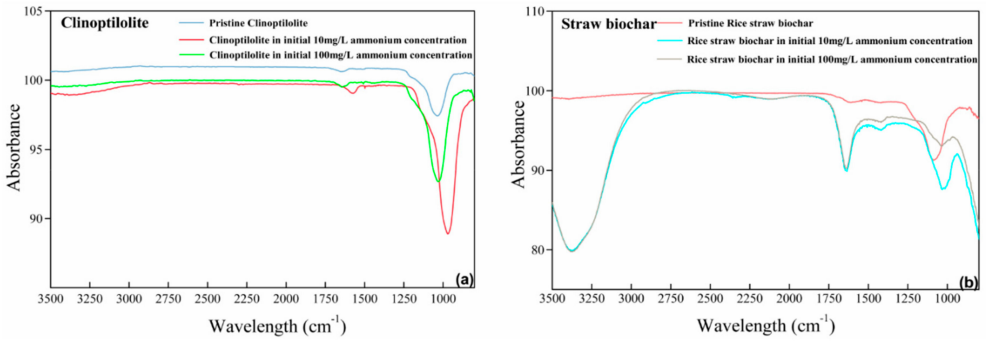

Figure 7. FTIR spectra of pristine materials and after the adsorption (**a**) Clinoptilolite; (**b**) Rice straw biochar.

3.2. *Ammonium Adsorption Kinetics of Different Adsorbents*

Langmuir adsorption isotherm was utilized to demonstrate the equilibrium between the adsorbent and adsorbed material (i.e. biochar and ammonium). This isotherm is seen to best fit the equilibrium data (with all adjusted $R^2 > 0.91$), indicating the homogeneous adsorption of ammonium into the surface of the biochar (Figure 8).

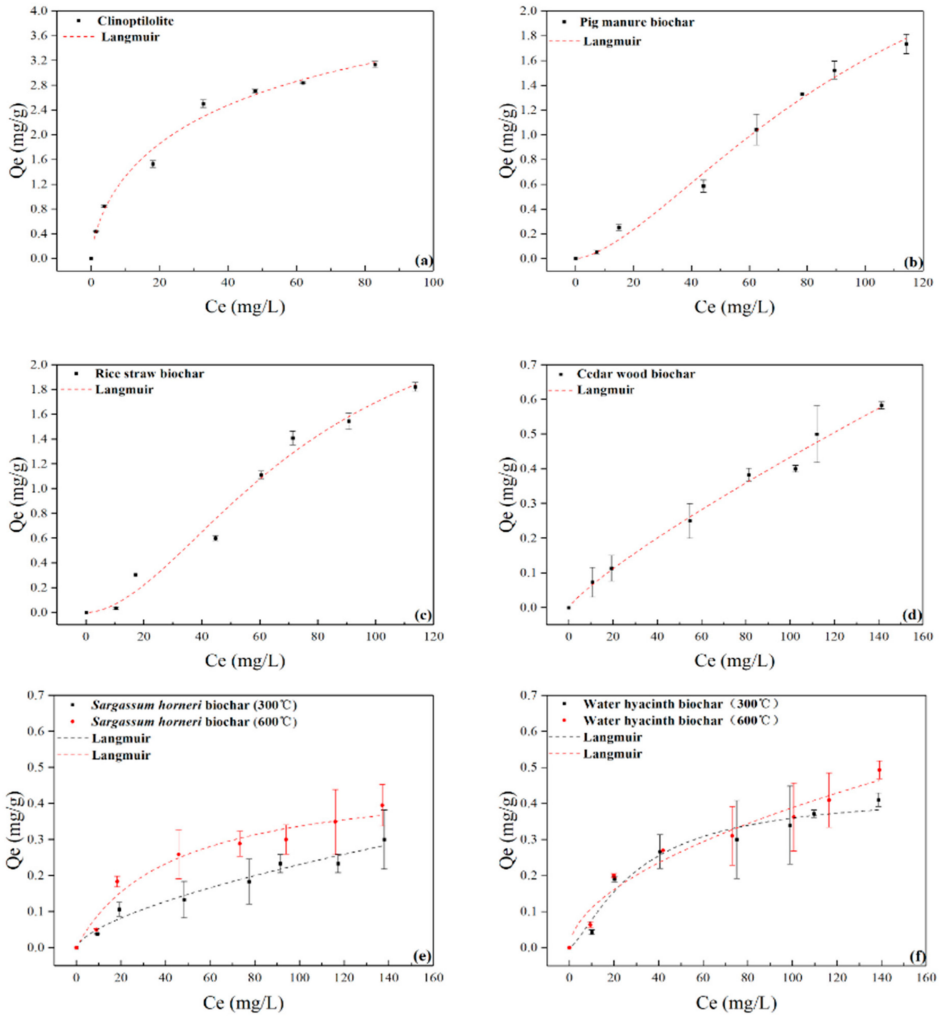

Figure 8. Adsorption isotherms curves of different materials such as (**a**) Clinoptilolite; (**b**) pig manure biochar; (**c**) rice straw biochar; (**d**) cedar wood biochar; (**e**) *Sargassum horneri* (300 °C) and *Sargassum horneri* (600 °C) biochar; (**f**) water hyacinth (300 °C) and water hyacinth (600 °C) biochar.

4. Conclusions

This study demonstrates the effect of different biochar types (from agricultural residue, wood, animal-based, and aquatic species), as well as pyrolysis temperature (for biochars from aquatic species) on adsorption capacity for ammonium nitrogen. An attempt was made to interpret adsorption mechanism of all biochars using their micro-structural analyses (SEM, XRD, and FTIR). The results of adsorption capacity for all biochars were compared with that of commercial clinoptilolite.

Clinoptilolite has the highest adsorption capacity in both low and highly concentrated ammonium solutions. It can be therefore used as a standard reference adsorbent to quantify effects of the newly developed biochar. Pig manure (animal-based) biochar has the highest adsorption capacity, followed by agricultural residues based (rice straw) biochar and wood-based biochar. Among all biochars, aquatic-based biochars have the lowest adsorption capacity. The capacity of pig manure biochar increases significantly under a highly concentrated ammonium solution (100 mg/L) and is merely 20% lower than that of clinoptilolite. Both water hyacinth and algae biochar produced at higher temperatures shows higher sorption rate and capacity (depending on the initial concentration of ammonium) for ammonium as compared to that produced at lower temperatures. This is likely due to an increase in porosity at higher pyrolysis temperature. Further, comparison of expenditure incurred during production of biochars needs to be conducted to carry out cost-benefit analysis for using various biochars in different applications (wastewater treatment at certain scale). In addition, systematic studies need to be conducted to quantify any possible leaching from biochars (especially produced at pyrolysis temperature ~ 300 °C).

Author Contributions: Funding acquisition, H.S. and A.G.; Investigation, J.W. and Q.Z.; Methodology, J.W., X.L. and Q.Z.; Supervision, H.S. and A.G.; Validation, S.S.; Writing–original draft, H.S. and J.W.; Writing–review & editing, A.G. and H.S.

Funding: Guangdong Science and Technology Department: No. 2019B110205003; 180917124960518 & 2017A040403067; National Natural Science Foundation (NSFC): No. 41907252.

Acknowledgments: The authors would like to acknowledge Guangdong Province Department of Science and Technology for Key–Area Research and Development Program of Guangdong Province (No. 2019B110205003) and Program 180917124960518 & 2017A040403067 for financial assistance. Corresponding author would also like to thank National Natural Science Foundation (NSFC) Youth Grant (No. 41907252) for support. We would also like to acknowledge Prof Weizhou Chen from College of Science, Shantou University for guidance on biochar production from algae.

Conflicts of Interest: The authors declare no conflict of interest.

References

1. Zheng, Y.; Wang, B.; Wester, A.E.; Chen, J.; He, F.; Chen, H.; Gao, B. Reclaiming phosphorus from secondary treated municipal wastewater with engineered biochar. *Chem. Eng. J.* **2019**, *362*, 460–468. [CrossRef]
2. Schoeman, J.J.; Steyn, A. Nitrate removal with reverse osmosis in a rural area in South Africa. *Desalination* **2003**, *155*, 15–26. [CrossRef]
3. Samatya, S.; Kabay, N.; Yüksel, Ü.; Arda, M.; Yüksel, M. Removal of nitrate from aqueous solution by nitrate selective ion exchange resins. *React. Funct. Polym.* **2006**, *66*, 1206–1214. [CrossRef]
4. Ahmad, M.; Ahmad, M.; Usman, A.R.A.; Al-Faraj, A.S.; Abduljabbar, A.S.; Al-Wabel, M.I. Biochar composites with nano zerovalent iron and eggshell powder for nitrate removal from aqueous solution with coexisting chloride ions. *Envrion. Sci. Pollut. Res.* **2018**, *25*, 25757–25771. [CrossRef] [PubMed]
5. Adeleye, A.S.; Conway, J.R.; Garner, K.; Huang, Y.; Su, Y.; Keller, A.A. Engineered nanomaterials for water treatment and remediation: Costs, benefits, and applicability. *Chem. Eng. J.* **2016**, *286*, 640–662. [CrossRef]
6. Tyagi, S.; Rawtani, D.; Khatri, N.; Tharmavaram, M. Strategies for Nitrate removal from aqueous environment using Nanotechnology: A Review. *J. Water Process Eng.* **2018**, *21*, 84–95. [CrossRef]
7. Bhatnagar, A.; Sillanpaa, M. A review of emerging adsorbents for nitrate removal from water. *Chem. Eng. J.* **2011**, *168*, 493–504. [CrossRef]
8. Wang, B.; Gao, B.; Fang, J. Recent advances in engineered biochar productions and applications. *Crit. Rev. Environ. Sci. Technol.* **2017**, *47*, 2158–2207. [CrossRef]

9. Xiao, Y.A.; Yang, S.H.; Xu, J.Z.; Ding, J.; Sun, X.; Jiang, Z.W. Effect of biochar amendment on methane emissions from paddy field under water-saving irrigation. *Sustainability* **2018**, *10*, 1371. [CrossRef]
10. Nguyen, M.-V.; Lee, B.-K. Removal of dimethyl sulfide from aqueous solution using cost-effective modified chicken manure biochar produced from slow pyrolysis. *Sustainability* **2015**, *7*, 15057–15072. [CrossRef]
11. Qi, L.; Niu, H.-D.; Zhou, P.; Jia, R.-J.; Gao, M. Effects of biochar on the net greenhouse gas emissions under continuous flooding and water-saving irrigation conditions in paddy soils. *Sustainability* **2018**, *10*, 1403. [CrossRef]
12. Gaskin, J.; Steiner, C.; Harris, K.; Das, K.C.; Bibens, B. Effect of low-temperature pyrolysis conditions on biochar for agricultural use. *Trans. Asabe* **2008**, *51*, 2061–2069. [CrossRef]
13. Sohi, S.P.; Krull, E.; Lopez-Capel, E.; Bol, R. Chapter 2—A review of biochar and its use and function in soil. In *Advances in Agronomy*; Academic Press: Cambridge, MA, USA, 2010; Volume 105, pp. 47–82.
14. Laird, D.A.; Fleming, P.; Davis, D.D.; Horton, R.; Wang, B.; Karlen, D.L. Impact of biochar amendments on the quality of a typical Midwestern agricultural soil. *Geoderma* **2010**, *158*, 443–449. [CrossRef]
15. Jayawardhana, Y.; Kumarathilaka, P.; Herath, I.; Vithanage, M. Chapter 6—Municipal solid waste biochar for prevention of pollution from landfill leachate. In *Environmental Materials and Waste*; Prasad, M.N.V., Shih, K., Eds.; Academic Press: Cambridge, MA, USA, 2016; pp. 117–148.
16. Li, J.H.; Li, L.; Chen, R.; Li, D.Q. Cracking and vertical preferential flow through landfill clay liners. *Eng. Geol.* **2016**, *206*, 33–41. [CrossRef]
17. Suliman, W.; Harsh, J.B.; Abu-Lail, N.I.; Fortuna, A.-M.; Dallmeyer, I.; Garcia-Perez, M. Influence of feedstock source and pyrolysis temperature on biochar bulk and surface properties. *Biomass Bioenergy* **2016**, *84*, 37–48. [CrossRef]
18. Xu, Y.; Chen, B. Investigation of thermodynamic parameters in the pyrolysis conversion of biomass and manure to biochars using thermogravimetric analysis. *Bioresour. Technol.* **2013**, *146*, 485–493. [CrossRef]
19. Zhang, P.; Sun, H.; Yu, L.; Sun, T. Adsorption and catalytic hydrolysis of carbaryl and atrazine on pig manure-derived biochars: Impact of structural properties of biochars. *J. Hazard. Mater.* **2013**, *244–245*, 217–224. [CrossRef]
20. Gao, F.; Xue, Y.; Deng, P.; Cheng, X.; Yang, K. Removal of aqueous ammonium by biochars derived from agricultural residuals at different pyrolysis temperatures. *Chem. Speciat. Bioavailab.* **2015**, *27*, 92–97. [CrossRef]
21. Shin, J.; Choi, E.; Jang, E.; Hong, S.; Lee, S.-R.; Balasubramani, R. Adsorption characteristics of ammonium nitrogen and plant responses to biochar pellet. *Sustainability* **2018**, *10*, 1331. [CrossRef]
22. Khalil, A.; Sergeevich, N.; Borisova, V. Removal of ammonium from fish farms by biochar obtained from rice straw: Isotherm and kinetic studies for ammonium adsorption. *Adsorpt. Sci. Technol.* **2018**, *36*, 1294–1309. [CrossRef]
23. Li, Z.; Delvaux, B. Phytolith-rich biochar: A potential Si fertilizer in desilicated soils. *GCB Bioenergy* **2019**, *11*, 1264–1282. [CrossRef]
24. Li, Z.; Delvaux, B.; Yans, J.; Dufour, N.; Houben, D.; Cornelis, J.-T. Phytolith-rich biochar increases cotton biomass and silicon-mineralomass in a highly weathered soil. *J. Plant Nutr. Soil Sci.* **2018**, *181*, 537–546. [CrossRef]
25. Houben, D.; Evrard, L.; Sonnet, P. Beneficial effects of biochar application to contaminated soils on the bioavailability of Cd, Pb and Zn and the biomass production of rapeseed (*Brassica napus* L.). *Biomass Bioenergy* **2013**, *57*, 196–204. [CrossRef]
26. Xu, X.; Cao, X.; Zhao, L.; Wang, H.; Yu, H.; Gao, B. Removal of Cu, Zn, and Cd from aqueous solutions by the dairy manure-derived biochar. *Environ. Sci. Pollut. Res.* **2013**, *20*, 358–368. [CrossRef] [PubMed]
27. Houben, D.; Sonnet, P. Impact of biochar and root-induced changes on metal dynamics in the rhizosphere of *Agrostis capillaris* and *Lupinus albus*. *Chemosphere* **2015**, *139*, 644–651. [CrossRef]
28. Yang, X.; Liu, J.; McGrouther, K.; Huang, H.; Lu, K.; Guo, X.; He, L.; Lin, X.; Che, L.; Ye, Z.; et al. Effect of biochar on the extractability of heavy metals (Cd, Cu, Pb, and Zn) and enzyme activity in soil. *Environ. Sci. Pollut. Res.* **2016**, *23*, 974–984. [CrossRef]
29. Mansouri, N.; Rikhtegar, N.; Panahi, H.; Atabi, F.; Karimi Shahraki, B. Porosity, characterization and structural properties of natural zeolite—Clinoptilolite—As a sorbent. *Environ. Prot. Eng.* **2013**, *39*, 139–152. [CrossRef]
30. Huang, Y.-F.; Chiueh, P.-T.; Shih, C.-H.; Lo, S.-L.; Sun, L.; Zhong, Y.; Qiu, C. Microwave pyrolysis of rice straw to produce biochar as an adsorbent for CO_2 capture. *Energy* **2015**, *84*, 75–82. [CrossRef]

31. Carrier, M.; Hardie, A.; Uras, Ü.; Görgens, J.; Knoetze, H. Production of char from vacuum pyrolysis of South-African sugar cane bagasse and its characterization as activated carbon and biochar. *J. Anal. Appl. Pyrolysis* **2012**, *96*, 24–32. [CrossRef]
32. Escobar, B.; Pérez-Salcedo, K.Y.; Alonso-Lemus, I.L.; Pacheco, D.; Barbosa, R. N-doped porous carbon from Sargassum spp. as metal-free electrocatalysts for oxygen reduction reaction in alkaline media. *Int. J. Hydrog. Energy* **2017**, *42*, 30274–30283. [CrossRef]
33. Wang, H.; Xia, W.; Lu, P. Study on adsorption characteristics of biochar on heavy metals in soil. *Korean J. Chem. Eng.* **2017**, *34*, 1867–1873. [CrossRef]
34. Garg, A.; Bordoloi, S.; Ni, J.; Cai, W.; Maddibiona, P.G.; Mei, G.; Poulsen, T.G.; Lin, P. Influence of biochar addition on gas permeability in unsaturated soil. *Geotech. Lett.* **2019**, *9*, 66–71. [CrossRef]
35. Kumar, H.; Ganesan, S.P.; Bordoloi, S.; Sreedeep, S.; Lin, P.; Mei, G.; Garg, A.; Sarmah, A.K. Erodibility assessment of compacted biochar amended soil for geo-environmental applications. *Sci. Total Environ.* **2019**, *672*, 698–707. [CrossRef] [PubMed]
36. Huang, H.; He, L.; Zhang, Z.; Lei, Z.; Liu, R.; Zheng, W. Enhanced biogasification from ammonia-rich swine manure pretreated by ammonia fermentation and air stripping. *Int. Biodeterior. Biodegrad.* **2019**, *140*, 84–89. [CrossRef]
37. Lahav, O.; Schwartz, Y.; Nativ, P.; Gendel, Y. Sustainable removal of ammonia from anaerobic-lagoon swine waste effluents using an electrochemically-regenerated ion exchange process. *Chem. Eng. J.* **2013**, *218*, 214–222. [CrossRef]
38. Halajnia, A.; Oustan, S.; Najafi, N.; Khataee, A.R.; Lakzian, A. Adsorption–desorption characteristics of nitrate, phosphate and sulfate on Mg–Al layered double hydroxide. *Appl. Clay Sci.* **2013**, *80–81*, 305–312. [CrossRef]
39. Sarkhot, D.; Ghezzehei, T.; Berhe, A. Effectiveness of biochar for sorption of ammonium and phosphate from dairy effluent. *J. Environ. Qual.* **2013**, *42*, 1545–1554. [CrossRef]
40. Sika, M.P.; Hardie, A.G. Effect of pine wood biochar on ammonium nitrate leaching and availability in a South African sandy soil. *Eur. J. Soil Sci.* **2014**, *65*, 113–119. [CrossRef]
41. Bordoloi, S.; Hussain, R.; Gadi, V.K.; Bora, H.; Sahoo, L.; Karangat, R.; Garg, A.; Sreedeep, S. Monitoring soil cracking and plant parameters for a mixed grass species. *Géotechnique Lett.* **2018**, *8*, 49–55. [CrossRef]
42. Bordoloi, S.; Garg, A.; Sreedeep, S.; Lin, P.; Mei, G. Investigation of cracking and water availability of soil-biochar composite synthesized from invasive weed water hyacinth. *Bioresour. Technol.* **2018**, *263*, 665–677. [CrossRef]
43. Gale, N.V.; Sackett, T.E.; Thomas, S.C. Thermal treatment and leaching of biochar alleviates plant growth inhibition from mobile organic compounds. *PeerJ* **2016**, *4*, e2385. [CrossRef] [PubMed]
44. Lievens, C.; Mourant, D.; Gunawan, R.; Hu, X.; Wang, Y. Organic compounds leached from fast pyrolysis mallee leaf and bark biochars. *Chemosphere* **2015**, *139*, 659–664. [CrossRef] [PubMed]
45. Yao, Y.; Gao, B.; Zhang, M.; Inyang, M.; Zimmerman, A.R. Effect of biochar amendment on sorption and leaching of nitrate, ammonium, and phosphate in a sandy soil. *Chemosphere* **2012**, *89*, 1467–1471. [CrossRef] [PubMed]